Renewable Energy 218 (2023) 119250

Contents lists available at ScienceDirect

Renewable Energy

journal homepage: www.elsevier.com/locate/renene

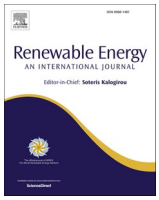

Monitoring of the thermal plume around a thermally activated borehole heat exchanger and characterization of the ground hydro-geothermal parameters

Valériane Gigot [a,b], Bertrand Francois [a,c], Marijke Huysmans [b], Pierre Gerard [a,*]

[a] Université libre de Bruxelles (ULB), Building, Architecture and Town Planning Dept (BATir), Laboratoire de GéoMécanique, Avenue F.D. Roosevelt, 50 – CPI 194/2, B – 1050, Brussels, Belgium
[b] Department of Hydrology and Hydraulic Engineering, Vrije Universiteit Brussel, Pleinlaan 2, 1050, Brussels, Belgium
[c] Université de Liège, Département ArGEnCo - Géotechnique, Géomécanique et Géologie de l'Ingénieur, Liège 1, 4000, Belgium

ARTICLE INFO

Keywords:
Borehole heat exchanger
Groundwater flux
Temperature plume
Experimental platform
Analytical solution
Intrinsic thermal conductivity

ABSTRACT

A methodology to characterize the main hydro-geothermal parameters of saturated and unsaturated ground layers, such as intrinsic thermal conductivity, volumetric heat capacity and groundwater velocity is proposed, based on the monitoring of the temperature plume around an activated borehole heat exchanger (BHE). The methodology is applied on an experimental platform composed of four BHEs. Based on the expected lithology and approximative groundwater fluxes direction, one BHE is thermally activated with a pre-determined heat injection and duration. The temperature evolution is recorded by means of PT100 sensors in the activated BHE and in the three non-activated BHEs, at three different depths in the saturated and unsaturated domain of an unconfined aquifer crossed by the BHEs. From an analytical solution considering conductive, advective and dispersive heat transfers, the hydro-geothermal parameters of the ground are obtained by fitting the measured to the predicted temperatures evolution. The effect of the possible inclination of the measuring boreholes is evaluated with the analytical solution. The obtained hydro-geothermal parameters demonstrate the important role of the saturated aquifer that significantly enhances the apparent thermal conductivity of the ground and, in case of groundwater flows, induces an anisotropic propagation of the temperature plume.

1. Introduction

Amongst the different technologies of shallow geothermal energy, closed-loop systems consist in circulating a heat-carrier fluid within borehole heat exchangers (BHEs). BHEs mainly consist in U-shaped, or less frequently co-axial, pipes buried into the ground and surrounded with grout. As the fluid circulates within the pipe, its temperature stabilizes with the ground temperature. Therefore, this method allows to warm up buildings during winters and to cool them down during summers [1–4].

The heat exchanges between ground and BHE can be significantly affected by the presence of groundwater. Larger conductive heat flows are expected in the saturated domain, since the intrinsic thermal conductivity of the ground is higher than under partially saturated conditions [5,6]. Besides, the volumetric heat capacity of the ground is also positively linked to its degree of saturation [7]. In addition, if groundwater fluxes take place, heat transfers by advection and dispersion also occur [8,9]. The presence of an aquifer may thus have a substantial impact on the performance of BHEs. The impact of groundwater fluxes has been already studied several times numerically [10–16] and analytically [17–21]. [22]; proposed an interesting review on that purpose. On the other hand, only few in-situ experiments highlighted the impact of groundwater flow [23,24]. There is consequently a significant interest to develop experimental methodologies allowing to infer the groundwater fluxes along BHEs, but also to characterize the impact of groundwater fluxes on heat transfers around BHEs.

Nowadays, the current dimensioning methods of BHEs fields are mainly based on the results of an in-situ Thermal Response Test (TRT) [25] or tests based on the same working principles [26]. The interpretation of TRTs is generally based on the Infinite Line Source (ILS) model

* Corresponding author.
E-mail addresses: valeriane.gigot@ulb.be (V. Gigot), bertrand.francois@ulb.be (B. Francois), marijke.huysmans@vub.be (M. Huysmans), gerard.pierre@ulb.be (P. Gerard).

https://doi.org/10.1016/j.renene.2023.119250
Received 23 November 2022; Received in revised form 22 August 2023; Accepted 29 August 2023
Available online 30 August 2023

proposed by Ref. [27]. This model considers that only conductive heat exchanges take place, leading to only radial heat transfers. Therefore, in presence of groundwater flows, the data from TRT analyzed from the ILS model only provide an apparent thermal conductivity, including the distinct heat transfer mechanisms (conduction, advection, dispersion) into a single one [28]. It is therefore not possible with this approach to distinguish and quantify straightforwardly the intrinsic thermal conductivity of the ground nor the groundwater flows, except under very high groundwater velocities for which the time required to reach a steady state temperature is compatible with the duration of standard TRT [29]. Some attempts have been done to develop specific experimental methods able to characterize the groundwater fluxes in fractured rocks based on the evolution of the vertical profile of the heat-carrier fluid temperature along a heated BHE, recorded by means of optic fibers or temperature probes. In fractured rocks, non-uniform temperature vertical profiles allow first to localize hydraulically active fractures and then to quantify the groundwater velocities, and also their directions [30–35]. However, those techniques can be applied only in geological conditions with high contrasts in the vertical distribution of the groundwater fluxes, which prevents their application in more homogeneous soil aquifers.

Besides, only a few studies proposed an experimental monitoring of the thermal plume around one or several BHEs under groundwater fluxes, and their results are generally not used to infer the ground hydrogeothermal parameters [36,37]. equipped multi-BHEs fields with temperature sensors installed along each BHE. After the activation of one or several BHEs, the measurement of the temperature evolution in the neighboring non-activated BHEs allowed them to characterize the migration of the thermal plume. Alternatively, Hermans et al. [38] deduced the ground temperature distribution around an activated BHE through electrical resistance tomography.

Facing the lack of experimental in-situ techniques to identify the distinct effect of heat conduction and advection for low to moderate groundwater fluxes, this paper proposes a methodology to characterize the intrinsic thermal conductivity and groundwater velocity, based on the monitoring of the temperature plume around an activated BHE. The first contribution of this paper is thus the monitoring of the temperature field evolution during the activation of a BHE. This is done from an existing experimental platform made up of four 85 m long BHEs crossing an unconfined aquifer. The second contribution is the elaboration of a methodology to characterize the groundwater fluxes (i.e. velocity and direction), the ground volumetric heat capacity and the intrinsic ground thermal conductivity based on the thermal plume measurements at different depths in both activated and non-activated BHEs, in both saturated and unsaturated domains of the unconfined aquifer. The physically based methodology rests upon the use of an existing analytical solution [39,40] able to predict the temperature evolution of the heat carrier fluid and the surrounding ground around an activated BHE in presence of groundwater fluxes and discontinuous heat injection/extraction. The methodology is validated through the comparison between the predictions and the monitored temperature field around the heated BHE at different depths.

2. Analytical solution

The methodology proposed in this paper uses an existing analytical solution developed by Ref. [39]. This analytical solution simulates discontinuous heat injection/extraction in finite-length BHE systems surrounded by a homogeneous and infinite ground for conduction, advection and dispersion dominated heat transfers and allows to predict the temperature evolution in the ground in case of both single and multiple BHEs.

The analytical solution is based on the energy balance equation including heat conduction, advection, and dispersion:

$$\rho c_p \frac{\partial T}{\partial t} = div\left(\underline{\lambda}\, \overrightarrow{grad}\, T\right) - \vec{v}\rho_w c_w \vec{\nabla} T + s \qquad \text{Eq 1}$$

with ρc_p [J/m^{3}K] the volumetric heat capacity of the ground, T [K] the temperature, t [s] the time, $\vec{v}$ [m/s] the groundwater velocity, $\rho_w c_w$ [J/m^{3}K] the volumetric heat capacity of water and s a volumetric heat source [W/m^3].

The ground thermal conductivity tensor $\underline{\lambda}$ [W/mK] includes the impact of the heat dispersivity. If the groundwater fluxes are oriented towards x axis and if their velocity is v_x [m/s], the principal components of the thermal conductivity tensor become [41]:

$$\lambda_{xx} = \lambda + \omega_L \rho_w c_w v_x \qquad \text{Eq 2}$$

$$\lambda_{yy} = \lambda_{zz} = \lambda + \omega_T \rho_w c_w v_x \qquad \text{Eq 3}$$

with λ [W/mK] the intrinsic thermal conductivity of the porous medium (supposed isotropic) when there is no groundwater flow and ω_T and ω_L [m] the transverse and longitudinal dispersivity respectively. Various authors showed a strong correlation between the longitudinal and transverse dispersivities of a porous medium and the Peclet number [42–44]. Besides, the ratio between the longitudinal and transverse dispersivities is also linked to the groundwater velocity. In this study, a ratio of 0.1 between the transverse and the longitudinal dispersivities is assumed and the longitudinal dispersivity value was fixed to be 1m, in accordance with various studies [42,44–46].

To apply a discontinuous heat extraction/injection in time domain, one must consider series of successive rectangular heat pulses. With q_L the specific heat extraction rate per m of BHE [W/m] and P_e the period of heat extraction/injection, the rectangular heat extraction function $q_L(t)$ is defined as:

$$q_L(t) = \begin{cases} q_L \, for \, t \in [0, P_e] \\ 0 \, for \, t \notin [0, P_e] \end{cases} \qquad \text{Eq.4}$$

Posing the function $f(x,y,z,t)$ as follow [39,47]:

$$f(x,y,z,t) = \frac{1}{8\pi t\sqrt{\lambda_{xx}\lambda_{yy}}}\, exp\left(- \frac{\left(x - \frac{v\rho c_p}{\rho_w c_w} t\right)^2}{\frac{4\lambda_{xx} t}{\rho c_p}} - \frac{y^2}{\frac{4\lambda_{yy} t}{\rho c_p}} \right) \left(erf\left(\frac{z}{\sqrt{\frac{4\lambda_{zz} t}{\rho c_p}}} \right) - erf\left(\frac{z - H}{\sqrt{\frac{4\lambda_{zz} t}{\rho c_p}}} \right) \right) \qquad \text{Eq 5}$$

with H [m] the length of the BHE, x, y and z [m] the position of the observation point in an orthonormal system centered in the center of the BHE with x and y in the horizontal plane and z downwards, and with x the direction of the horizontal groundwater flows.

Then, by calculating the convolution product of $f(x,y,z,t)$ and $q_L(t)$ and by discretizing both functions with a differential of time Δt, the solution of the partial differential equation (Eq. (1)) can be expressed as the convolution of a sum of heat impulses responses at given coordinates and time (x,y,z,t) and is equal to:

$$\Delta T(x,y,z,t) = \sum_{i=0}^{p-1} q_L(i\Delta t) f(x,y,z,t - i\Delta t)\Delta t \qquad \text{Eq 6}$$

with p denoting the time span and $i\Delta t$ the time delay of each unit impulse. The delayed and shifted impulse response is thus $q_L(i\Delta t)f(t - i\Delta t)\Delta t$.

For a steady-state heat flux within the BHE, the average heat carrier fluid temperature T_f evolution can be then determined through [40,48]:

$$T_f(z,t) = T_b(z,t) + R_b\, q_L(t) \qquad \text{Eq. 7}$$

with T_b the temperature at the BHE wall calculated by Eq. (6), R_b [mK/W] is the BHE thermal resistance and q_L is the specific heat extraction rate per meter of BHE [W/m]. The BHE thermal resistance depends on the type of exchangers, the BHE diameter and spacing between the pipes, the thermal conductivity of the grout and the pipes. It can be deduced from various methods, like the analytical multipole method [49], the shape factor model [50], or by using an equivalent diameter of the BHE to consider the effects of the pipes within the BHE [51].

All the key parameters related to the hydro-geothermal properties of the ground and to the geometrical characteristics of the BHE used in this analytical model are displayed in Table 1. As mentioned earlier, the longitudinal and transverse dispersivity values are fixed. In addition, both length and diameter of the BHE are supposed to be known. The remaining unknown parameters are thus the volumetric heat capacity of the ground ρc_p, the thermal conductivity of the ground λ, the groundwater velocity v, the groundwater flow direction θ and the thermal resistance of the BHE R_b.

3. Experimental platform with monitored borehole heat exchangers

3.1. Experimental platform

An experimental platform made up of four 85 m long BHEs and one piezometer installed in Brussels, on the campus of Université libre de Bruxelles (ULB) (coordinates: 50.8146981,4.38287194), is used in this study. The relative location of the four BHEs and the piezometer are given in Fig. 1. They form a quadrangle, and are named F1, F2, F3 and F4. Each BHE is composed of 2 U-shaped pipes in which the heat carrier fluid (water) can circulate and can be thermally-activated individually. The piezometer depth is equal to 50 m.

The 3D-GIS geological model of the Brussels-Capital Region [52] is used to reconstruct the stratigraphic log below the experimental platform. The stratigraphy is displayed on Fig. 2 and was ascertained by the lithological description of the ground collected during the drilling of the piezometer. The geological model highlights the presence of horizontal sedimentary layers from the Cenozoic period. The ground consists in an alternation of clayey and sandy deposits. Fig. 2 highlights the presence of a 30 m thick unconfined aquifer in the Brusselian sand geological unit. The saturated thickness is around 17 m while the top 13 m are unsaturated. The screens of the piezometer are installed along this aquifer. The present study is exclusively focused on that geological unit (both saturated and unsaturated parts) in order to evaluate the impact of the groundwater fluxes on the thermal plume around an activated BHE and to investigate if the hydro-geothermal properties of the ground can be back-analyzed from the monitoring of the temperature field.

Based on existing piezometric maps of the Brussels-Capital region [53], a preliminary estimation of the direction of the groundwater fluxes in the Brusselian unconfined aquifer was deduced to be approximately

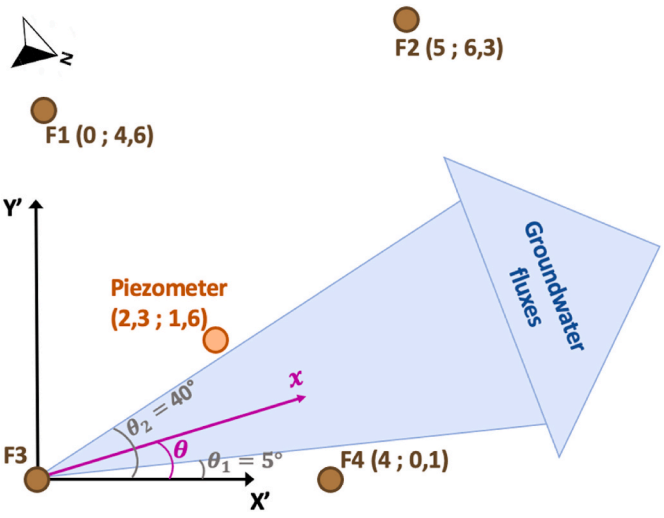

Fig. 1. *Top view of the experimental platform with relative position of the 4 BHEs (in meters) and preliminary estimation of the direction of the groundwater fluxes in the Brusselian aquifer θ, based on piezometric map. F3: Thermally-activated BHE; F1, F2 and F4: non-activated BHEs.*

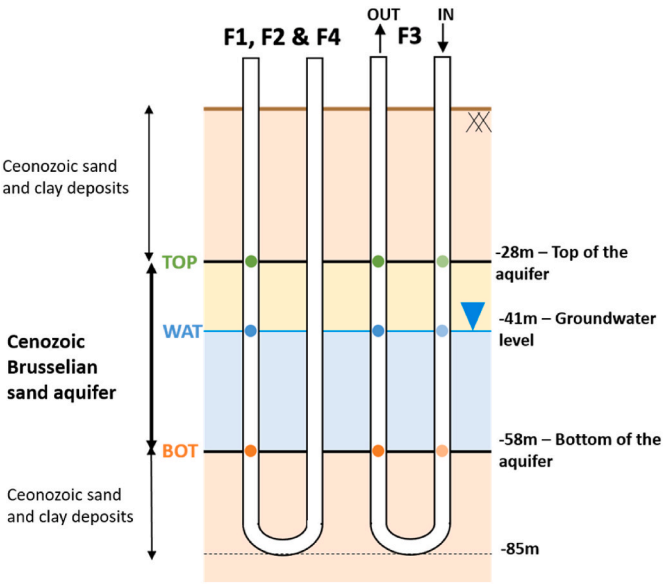

Fig. 2. Stratigraphy of the ground located below the experimental site and locations of temperature sensors along the BHEs.

between 326° and 331° from north (i.e., in the north-west direction). It is worth to note that this first estimation is prone to relatively large uncertainties because the site is located near a local piezometric crest in the Brusselian sand aquifer with relatively low hydraulic gradient. Consequently, the direction of the groundwater fluxes will be an unknown of the model, and a total safety margin of +/- 15° will be considered (i.e., in the range of 5°–40° compared to the x' axis between F3 and F4, as plotted in Fig. 1).

Because of the expected direction of the groundwater fluxes in the Brusselian sand aquifer, it was decided to thermally-activate the BHE located at the upstream zone of the site (i.e., F3), while the three other BHEs (i.e., F1, F2 and F4) will be used as measuring BHEs to monitor the migration of the thermal plume.

Table 1
Input parameters of the analytical solution (unknowns are underlined).

	Parameter	Units
Ground hydro-geothermal parameters	Intrinsic thermal conductivity of the ground, λ	W/mK
	Volumetric heat capacity of the ground, ρc_p	J/m^{3}K
	Groundwater velocity, v	m/s
	Groundwater direction, θ	°
	Longitudinal Dispersivity, ω_L	m
	Transverse dispersivity, ω_T	m
Geometrical characteristics of the BHE	BHE length, H	m
	Resistance of the BHE, R_b	mK/W
	Diameter of the BHE, D_b	m

3.2. Temperature monitoring system

The focus being on the hydro-geothermal behavior of the Brusselian sand aquifer, it was decided to monitor the temperature evolution at the top and bottom of the Brusselian sand aquifer and just below the groundwater table level, as reported in Fig. 2. In the following, the three levels will be called TOP, WAT and BOT for the top of the Brusselian sand unit, the level of the groundwater table and the bottom of the Brusselian sand unit, respectively. Consequently, three temperature sensors were inserted in the pipes of the four BHEs to reach those three levels. For the three non-activated BHEs (F1, F2 and F4), sensors were inserted in one of the outlets of the BHE. In the activated BHE, temperature sensors were inserted in both the inlet and the outlet of the same pipe. Because of the relatively long horizontal distance between some sensors installed at the same depth (more than 7,5m between F2 and F3) and the duration of the heating phase of a few months, the temperature evolution in some non-activated BHEs was expected to be lower than 0,5 °C. In other words, there was a need to find sensors accurate enough to detect temperature variations as small as 0,2-0,3 °C and with a diameter thin enough to insert 3 of them in the pipes, whose inner diameter is 26 mm. For this reason, class 1/10 PT100 were selected. Their accuracy is ± (0,03 °C + 0,5%). A Fluke 2638A Hydra Serie III multimeter was used to measure the resistance variation. The total accuracy of the apparatus (PT100 and multimeter) was considered to be equal to 0,1 °C. To record the temperature evolution in the activated BHE when heated water is circulating within the pipe, the watertightness of the system should be ensured even after the insertion of the sensors. To do so, a T-shaped tool was developed, as shown in Fig. 3.

4. Methodology

4.1. General layout

In this section, the procedure proposed to determine the hydro-geothermal parameters of the ground from the experimental characterization of the heat plume around an activated BHE is described. This procedure is first based on the monitoring of temperature at three different depths in the activated BHE and the three non-activated BHEs. Heat is injected through a surface heat pump in the activated BHE and the temperature evolution is monitored in the four BHEs. Then the hydro-geothermal parameters are calibrated using the analytical solution to fit the monitored temperatures.

Fig. 3. T-shaped pipe tool ensuring the watertightness of the system and an alteration as limited as possible of the fluid flow within the U-shaped pipe.

Step 1 of the procedure is to design the heat load and the duration of the heat injection in the activated BHE in order to induce a temperature plume that can be detected in the non-activated BHEs in a realistic duration of the heating phase (i.e., the order of a couple of months). Step 2 of the procedure consists in performing a sensitivity analysis of the impact on the temperature evolution in both activated and non-activated BHEs of each unknown enumerated in Table 1. During this second step, the range of variation of the unknowns is kept in realistic values, as a function of the lithology and the hydrogeological context. The sensitivity analysis aims at discriminating the unknowns that significantly affect the temperature response at the activated BHE from those ones that impact the temperature mainly in the non-activated BHEs. Thanks to the discrimination of the parameters, the final calibration (Step 3) can be performed in two phases from the knowledge of the temperature field: (i) calibration of the parameters affecting the temperature evolution in the activated BHE (step 3a of the procedure), followed by (ii) calibration of the remaining parameters from the non-activated BHEs, keeping the parameters determined in step 3a unchanged (step 3b of the procedure). This strategy allows to reduce the number of unknowns in each calibration phase. Steps 3a and 3b must be repeated for the three depths of investigation in order to obtain the hydro-geothermal properties of both saturated and unsaturated zone of the Brusselian aquifer.

4.2. Step 1: design of the heat load

The heat load and duration of the heat injection must be designed such that the induced temperature variation in the farthest non-activated BHE (i.e., F2) is reached with a magnitude larger than the accuracy of the temperature sensor. The analytical solution was used in that purpose, using realistic ranges of hydro-geothermal parameters of the ground. The lowest expected temperature variation in F2 was at the TOP level, as this level is above the groundwater level (i.e., in the unsaturated part of the aquifer). Preliminary values of the thermal conductivity of 1,0 W/mK and volumetric heat capacity of the ground of 2,2 MJ/m^3K were used for first simulations, with no groundwater flow. When a heat load of 59 W/m is applied at BHE during 65 days and then stopped, the maximal temperature variation in the farthest non-activated BHE (7.5 m away from the activated BHE) was maximal after 250 days, and close to 0,25 °C. Such a heat load (i.e., 59 W/m) is in the usual order of magnitude for standard TRTs [54,55].

Instead of that monotonic heat load, we decided to apply a discontinuous thermal response test made of two successive thermal loading phases, separated by a recovery period. This allows to have access to the thermal response of the ground during recovery and restart periods. This two-phases heating allows also to adjust eventually the thermal power of the second heating phase based on the observation of the first heating period. Also, the duration of the recovery period between the two heating phases was tuned as a function of the temperature monitoring data. We started the second heating phase when the temperature variation in the activated BHE was come back at less than 1 °C (while the peak of temperature variation at the end of the first heating phase was 22 °C).

Finally, based on the preliminary modelling and the adjustment during the test, the heat load was designed as follow. The first thermal loading phase, called TRT A, lasts 11,5 days with a fixed injected heat q_L of 68 W/m. Then a recovery period of 22 days was imposed during which no thermal load was applied, followed by the second heating phase (called TRT B) that lasts 87 days with a heat injection q_L of 45 W/m. Finally, after the second heating phase, a recovery period of 120 days was maintained, during which temperatures were still monitored while the heating was stopped.

4.3. Step 2: preliminary sensitivity analysis

Based on the lithology of Brusselian unconfined aquifer (i.e., sand), Belgian recommendations [56,57] narrow the range of plausible values of volumetric heat capacity ρc_p and thermal conductivity λ of the ground, both in the saturated and unsaturated domains, as defined in Table 2. A specific test called Finite Volume Point Dilution Method (FVPDM), based on long-term tracer dilution [58,59], was performed in the piezometer available on the site to infer the groundwater velocity, that was determined equal to 8 10^{-7} m/s. Because the groundwater velocity is generally highly affected by the local heterogeneity of the hydraulic conductivity of the ground and the volume of ground characterized by the measurements, we selected a preliminary range of velocity between 8 10^{-8} m/s and 8 10^{-6} m/s. The plausible range of groundwater flux direction was deduced from piezometric maps of the Brussels-Capital region [53] and is shown on Fig. 1. Finally, using the analytical multipole method [49]; Hellström,1991) and the available technical data of the BHEs, the resistance of the BHE was narrowed in a range between 0,04 mK/W and 0,13 mK/W depending on the spacing between the pipes and the thermal conductivity of the grout that are not precisely known.

To reduce the number of ground parameters to calibrate based on the monitored temperatures, a sensitivity analysis is done to discriminate two categories of ground parameters, i.e. the parameters that essentially affect the temperature in the activated BHE and the parameters affecting the temperature in a farther field (i.e., in the non-activated BHEs). Based on the plausible range of unknowns as established in Table 2, the sensitivity analysis, performed through the analytical solution, reveals the relative impact of each parameter in both activated and non-activated BHEs, as illustrated in Table 3. For this sensitivity analysis, the non-activated BHE is assumed to be located at 4 m from the thermally activated BHE, in the direction of groundwater fluxes. Those relative impacts are coherent with the publications of previous authors [60,61].

4.4. Step 3: determination of ground hydro-geothermal parameters

Based on the outcomes of the sensitivity analysis, the calibration of the hydro-geothermal parameters of the ground is decomposed into two stages, i.e., step 3a (calibration based on the temperature monitored at the activated BHE) and step 3b (calibration based on the temperature evolution in non-activated BHEs). In step 3a, the thermal resistance of the BHE R_b, the thermal conductivity of the ground λ and the groundwater velocity v (when applicable) are determined. In step 3b, the monitored temperature at non-activated BHEs serves to calibrate the remaining unknowns: the volumetric heat capacity of the ground ρc_p and the groundwater flux direction θ (when applicable). Unlike steps 1 and 2, that are applied once, the two stages (3a and 3b) are applied successively for the three monitored depths, from the TOP level (i.e., the top boundary of the aquifer) to the BOT level (i.e., the bottom boundary of the aquifer). This sequencing was motivated as follows. Starting from the TOP level reduces the number of unknowns because the groundwater velocity is nul. Then, the thermal resistance of the BHE R_b determined at the TOP level will be considered constant along all the depth of the BHE, which allows to reduce the number of unknowns at the other levels where additional hydrogeological parameters must be considered (i.e. groundwater velocity v and direction θ). Finally, the saturated thermal conductivity of the ground λ_{sat}, the saturated volumetric heat capacity of the ground $\rho c_{p_{sat}}$ and the groundwater direction θ will be considered constant along the saturated part of the aquifer. This will not be the case for the groundwater velocity v. Indeed, as the hydraulic conductivity is highly heterogeneous within the Brusselian sandy aquifer [62,63], the groundwater velocity is expected to be heterogeneous along the thickness of the saturated part of the aquifer as well. The adopted procedure is summarized on Fig. 4, where the parameters considered as known, because either fixed or already determined in previous levels or steps, are highlighted in bold. It highlights that at BOT level, the prediction of the temperature field in the non-activated BHEs is a blind prediction, since all the ground parameters were determined in the previous stages.

Alternately to some existing methods developed for geothermal purposes and that propose an automated calibration of the hydro-geothermal parameters of the ground (Pasquier, 2015; Zhang et al., 2015; [64], we preferred to apply here a manual back-analysis of the parameters, based on a stepwise methodology that considers the specificity of the studied case, with the three monitored levels having connected and non-connected unknowns between the various levels. This stepwise methodology allows to reduce the high total number of hydro-geothermal parameters to determine into a limited number for every step. Also, the manual analysis allows to provide an in-depth physical understanding of the heat transfers around the activated BHE.

Table 2
Minimal and maximal values of the volumetric heat capacity ρc_p and thermal conductivity λ of the Brusselian aquifer [56], of the thermal resistance of the BHE R_b [48], of the direction of the groundwater fluxes θ [53], and of the groundwater velocity v (from FVPDM results).

		Minimal value	Maximal value
ρc_p (MJ/m^{3}K)	Unsat. sand	1,6	2,2
	Sat sand	2,2	2,8
λ (W/mK)	Unsat. sand	1,0	1,9
	Sat sand	2,0	3,0
R_b (mK/W)		0,04	0,13
θ (°)		5	40
v (m/s)		8 10^{-6}	8 10^{-8}

Table 3
Sensitivity analysis of the relative impact of each unknown in both activated and non-activated BHEs.

	At the activated BHE	4m from the activated BHE in the groundwater flux direction
Volumetric heat capacity of the ground, ρc_p	low	high
Resistance of the BHE, R_b	medium	nul
Thermal conductivity of the ground, λ	high	medium
Groundwater velocity, v	high	high
Groundwater direction, θ	nul	high

5. Results

In this section, we present the measured temperature evolutions at the different BHEs and depths in parallel with the temperature evolutions deduced from the analytical solution obtained after parameter calibration. For the activated BHE, the monitored temperature at a given depth is the average temperature between the inlet and outlet temperatures. The BHEs are assumed vertical.

5.1. Temperature evolution at the TOP level

At TOP level, the experimental temperature evolution at the activated BHE is reported in Fig. 5, highlighting the two successive heat injections (TRT A and TRT B). The temperature increase is higher and shorter during TRT A, while it is lower but longer during TRT B. The non-smooth temperature curve between day 50 and day 120 (i.e., during TRT B) are probably due to the outside temperature variation that alters the effective thermal power injected in the activated BHE due to heat loss in the pipes between the heat pump and the head of the activated BHE, as TRT B was performed during a cold winter.

The thermal resistance of the BHE R_b and the thermal conductivity of the unsaturated ground λ_{unsat} were first calibrated, based on the temperature evolution at the activated BHE (Step 3a). The groundwater

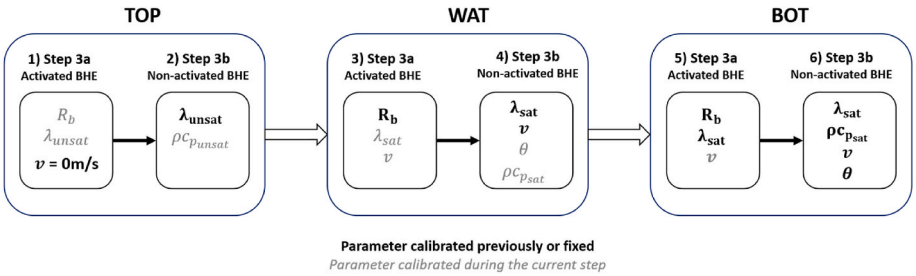

Fig. 4. Steps 3a and 3b - sequence of calibration of the different hydro-geothermal parameters at the three levels based on the adopted procedure.

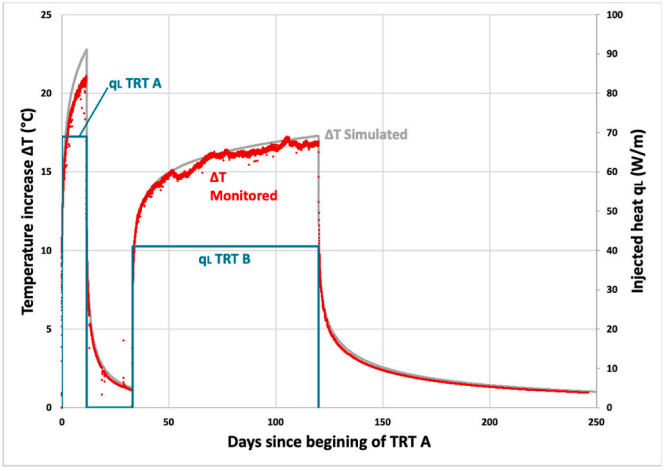

Fig. 5. Correlation between monitored and simulated temperature evolutions at the activated BHE, at the TOP level with $\lambda unsat = 1{,}9$ W/mK, $\rho c_{p,unsat} = 2{,}1$ MJ/m^{3}K, $R_b = 0{,}09$ mK/W and $v = 0$ m/s.

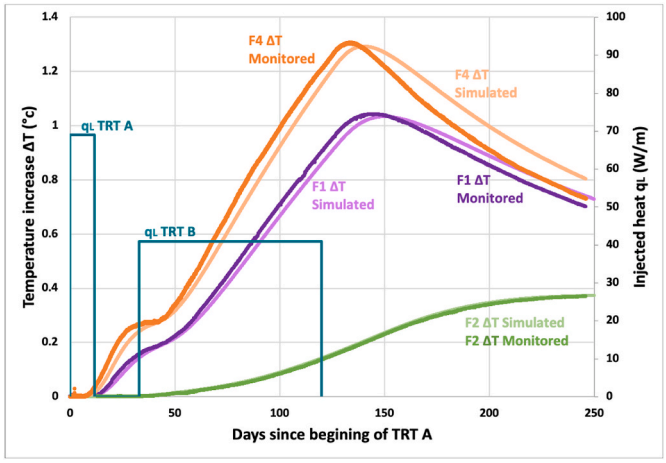

Fig. 6. Correlation between monitored and simulated temperature evolution in the 3 non-activated BHEs (F1, F2 and F4) at the TOP level with $\lambda unsat = 1{,}9$ W/mK, $\rho c_{p,unsat} = 1{,}8$ MJ/m^{3}K, $R_b = 0{,}09$ mK/W and $v = 0$ m/s.

velocity v is fixed to 0 m/s, as the TOP level is above the groundwater level. While keeping both R_b and λ_{unsat} in realistic ranges of values (Table 2), both parameters were determined in order to obtain the best agreement between the measured and predicted temperatures. An unsaturated thermal conductivity $\lambda_{unsat} = 1{,}9$ W/mK and a thermal resistance $R_b = 0{,}09$ mK/W were obtained, with a volumetric heat capacity that plays a minor role at the activated BHE $\rho c_{p,unsat} = 2{,}1$ MJ/m^{3}K.

During step 3b, the volumetric heat capacity of the ground $\rho c_{p,unsat}$ was more precisely characterized from the monitored temperatures at the non-activated BHEs. The best value of the volumetric heat capacity of the ground was thus calibrated to 1,8 MJ/m^{3}K, the other ground and BHE parameters (i.e., λ_{unsat} and R_b) remaining the same. This value is in the range of acceptable values displayed in Table 2. Both experimental and numerical temperatures for the 3 non-activated BHEs at the TOP level are displayed in Fig. 6. Similarly to the temperature curves in the activated BHE, both experimental and analytical results show a good agreement in the three non-activated BHEs. The maximal difference between them is observed at F4 and is around 0,08 °C (i.e., lower than the accuracy of the measurement system).

5.2. Temperature evolution at the WAT level

Similarly to the TOP level, steps 3a and 3b of the procedure were then applied at the WAT level (i.e. at the top of the saturated domain). The only differences are that, during step 3a, the groundwater velocity cannot be considered to be equal to 0 m/s and that the thermal resistance of the BHE is already known ($R_b = 0{,}09$ mK/W), since assumed constant all along the BHE. The temperature sensors are now located below the water table, and saturated thermal properties of the ground must thus be characterized. At this step 3a, the saturated thermal conductivity λ_{sat} and the groundwater velocity v were calibrated ($\lambda_{sat} = 2{,}4$ W/mK, $v = 3\ 10^{-7}$ m/s) while the other parameters that have minor or no effects at this step were fixed to some realistic values ($R_b = 0{,}09$ mK/W, $c_{p,sat} = 2{,}2$ MJ/m^{3}K and $\theta = 10°$). Fig. 7 shows the comparison between monitored and predicted temperatures, with better agreement during recovery periods than during heating periods. Nevertheless, the calibration quality seems to be slightly lower than at the TOP level, with a maximum relative error around 7% (i.e., absolute error about 1,2 °C) during heating phases.

The saturated volumetric heat capacity of the ground $\rho c_{p,sat}$ and the groundwater fluxes direction θ were then calibrated during step 3b of

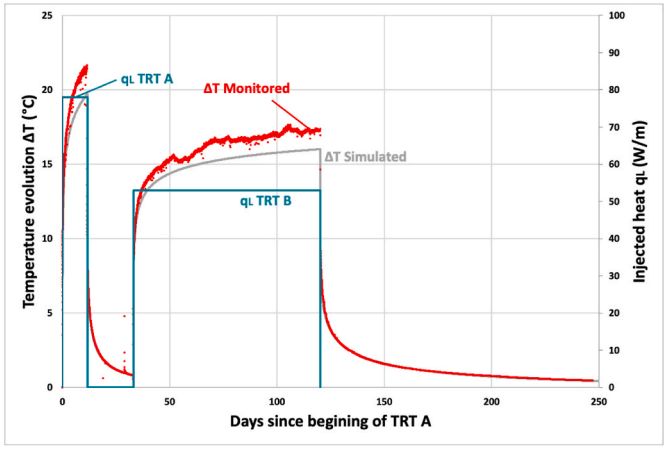

Fig. 7. Correlation between monitored and simulated temperature evolutions at the activated BHE, at the WAT level with $\lambda sat = 2{,}4$ W/mK, $\rho c_{p,sat} = 2{,}2$ MJ/m^{3}K, $R_b = 0{,}09$ mK/W, $\theta = 10°$ and $v = 3\ 10^{-7}$ m/s.

the procedure, based on the temperatures in the 3 non-activated BHEs at BOT level ($\rho c_{p,sat}$ = 2,2 MJ/m^{3}K and $\theta = 14°$, i.e. 322° from North). Both experimental and numerical temperature curves for the 3 non-activated BHEs at the WAT level are displayed in Fig. 8. The fitting between the experimental and the numerical temperature curves are very good in both F4 and F2. For F1, the difference between the measured and simulated temperatures is significantly higher (i.e., maximum relative error about 25%), even if the maximum absolute error remains limited (<0,3 °C). The effect of the groundwater velocity can be clearly noticed. Despite F1 and F4 are located at relatively similar distance from the activated BHE, the temperature variation is more pronounced in F4 than F1, because the groundwater flux is essentially directed toward F4.

To validate the calibration, it was also decided to perform a blind prediction of the temperature evolution within the piezometer at the WAT level, where a temperature sensor was inserted. Blind-predicted (with the same set of ground parameters used in Fig. 8) and experimental temperature evolutions are displayed in Fig. 9, showing the good matching between both curves and a good confidence in the hydro-geothermal parameters inferred for the WAT level.

5.3. Temperature evolution at the BOT level

The procedure was then applied at the bottom of the saturated domain (BOT level). At the activated BHE, only the groundwater velocity has to be determined, all the other ground parameters are supposed known from the previous steps (λ_{sat} = 2,4 W/mK, R_b = 0,09 mK/W, $\rho c_{p,sat}$ = 2,2 MJ/m^{3}K, $\theta = 14°$). According to the calibration, a null groundwater velocity (v = 0 m/s) provides the best matching at both activated and non-activated BHE, as displayed in Fig. 10. With those parameters, the maximum absolute error, occurring at the F4 BHE, is 0,2 °C, corresponding to a maximum relative error of 17%. The difference of groundwater velocity between the WAT and BOT levels ($v = 3\ 10^{-7}$ m/s and v = 0 m/s, respectively) corroborates the impact of the vertical heterogeneity of the hydraulic conductivity in the Brusselian aquifer. The null groundwater velocity at the bottom of the aquifer could be also explained by the possibility that the temperature sensors are very close to the transition zone between the Brusselian sandy aquifer and the underlying sand and clay Cenozoic layer (Fig. 2).

5.4. Consistency of the hydro-geothermal parameters of the ground

The hydro-geothermal parameters of the Brusselian aquifer determined in both saturated and unsaturated domains by means of the proposed procedure are summarized in Table 4. All those parameters are

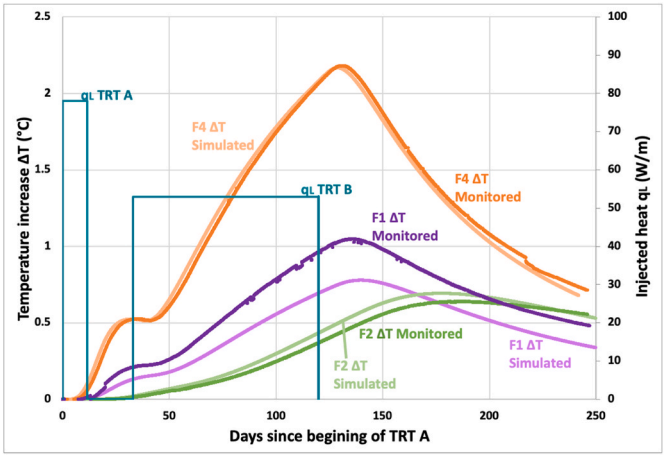

Fig. 8. Correlation between monitored and simulated temperature evolutions in the 3 non-activated BHEs (F1, F2 and F4), at the WAT level with λsat = 2,4 W/mK, $\rho c_{p,sat}$ = 2,2 MJ/m^{3}K, R_b = 0,09 mK/W, $\theta = 14°$ and $v = 3\ 10^{-7}$ m/s.

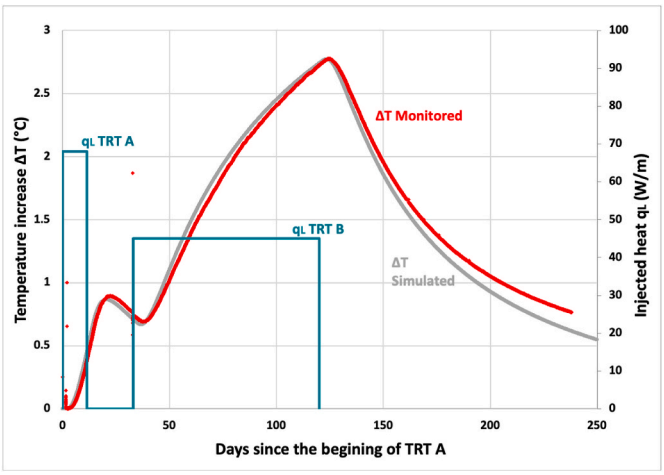

Fig. 9. Blind prediction of the temperature evolution in the piezometer, at the WAT level, with λsat = 2,4 W/mK, $\rho c_{p,sat}$ = 2,2 MJ/m^{3}K, R_b = 0,09 mK/W, $\theta = 14°$ and $v = 3\ 10^{-7}$ m/s, and comparison with experimental measurements.

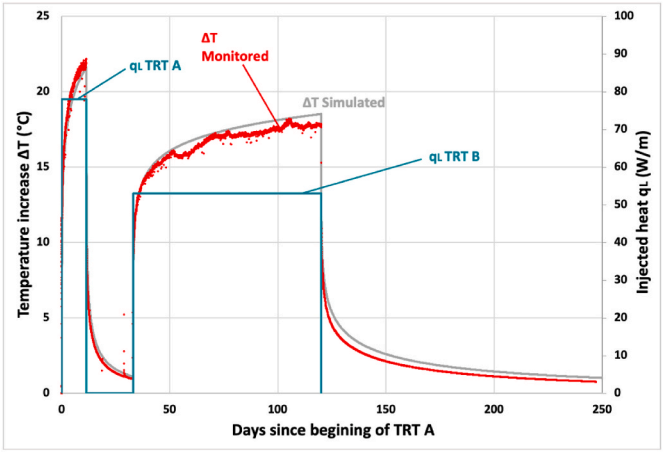

(a)

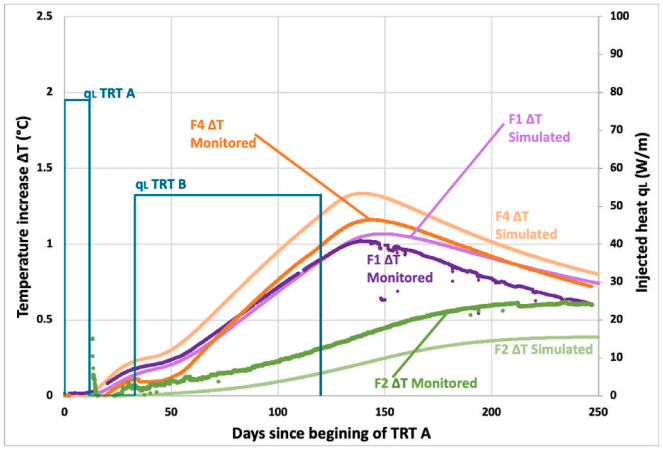

(b)

Fig. 10. Correlation between monitored and simulated temperature evolutions in the activated BHE (a) and in 3 non-activated BHEs (F1, F2 and F4)(b), at the BOT level with λ_{sat} = 2,4 W/mK, $\rho c_{p,sat}$ = 2,2 MJ/m3K, R_b = 0,09 mK/W and v = 0 m/s.

Table 4
Hydro-geothermal parameters of the ground in saturated and unsaturated domains.

	Unsaturated domain	Saturated domain
Resistance of the BHE, R_b [mK/W]	0,09	
Volumetric heat capacity of the ground, ρc_p [MJ/m^{3}K]	1,8	2,2
Thermal conductivity of the ground, λ [W/mK]	1,9	2,4
Groundwater velocity, v [m/s]	0	0–3 10^{-7}
Groundwater direction, θ [°]	/	14

in the ranges of plausible values as preliminary defined in Table 2.

The thermal conductivity and the volumetric heat capacity of the ground can be expressed as a function of the degree of saturation S_r and the porosity n as follow [5,65]:

$$\rho c_p = (1-n)\rho_s c_s + S_r n \rho_w c_w \quad \text{Eq. 8}$$

with $\rho_w c_w$ (= 4,18 MJ/m^{3}K) the volumetric heat capacity of water and $\rho_s c_s$ the volumetric heat capacity of the solid particles, that can be considered equal to 1,45 MJ/m^{3}K in a sandy aquifer (i.e., the average value of the volumetric heat capacity of sand particles according to Ref. [66].

$$\lambda = \lambda_s^{1-n} \lambda_w^{S_r n} \lambda_a^{(1-S_r)n} \quad \text{Eq. 9}$$

with λ_s the thermal conductivity of the solid particles [W/mK], λ_a (= 0,024 W/mK) the thermal conductivity of air and λ_w (= 0,598 W/mK) the thermal conductivity of water [67,68].

The thermal conductivity of the solid particles depends on the mineralogy of the soils. According to Ref. [67]; it can be decomposed into the thermal conductivity of the quartz minerals that are highly conductive (λ_q = 7,7 W/mK), and the thermal conductivity of the other minerals that has been averaged to $\lambda_{other\ min}$ = 2 W/mK. If q is the quartz content, the thermal conductivity of the geological material becomes:

$$\lambda = \left(7,7^q 2^{1-q}\right)^{1-n} \lambda_w^{S_r n} \lambda_a^{(1-S_r)n} \quad \text{Eq. 10}$$

According to Ref. [69]; the quartz content q in the Brusselian sandy aquifer is approximately 85%. Therefore, λ_s is equal to 6,29 W/mK.

Since the saturated volumetric heat capacity $\rho c_{p,sat}$ and saturated thermal conductivity λ_{sat} are known from the calibration procedure, the porosity can be inferred from Eqs. (8) and (10) for $S_r = 1$. From Eq. (8), it yields to n = 0,28, while from Eq. (10), it yields to n = 0,41. Then, if the porosity is assumed uniform all along the aquifer, the degree of saturation can be then determined at the top of the unsaturated domain. A degree of saturation S_r = 0,65 is obtained from Eq. (8), and S_r = 0,82 from Eq. (10). The procedure is illustrated in Fig. 11 and the values of porosities and degrees of saturation are summarized in Table 5.

Fig. 11 and Table 5 highlight that a single set of values of the porosity and degree of saturation cannot explain the calibrated thermal conductivities and volumetric heat capacities. However, according to the geotechnical maps of the area [70], the porosity of the Brusselian aquifer is between 0,19 and 0,52, with an average value of 0,39. The range of porosities inferred from our analysis (i.e., 0,28- 0,41) is thus realistic. For the degree of saturation, it does not exist any experimental data at a specific level in this aquifer, but the obtained range (i.e., 0,65-0,82) is narrow and quite realistic.

5.5. Impact of the deviation of the BHEs

The results presented in the previous sections reveal that the quality of the correlation between the simulated and monitored temperature evolutions tends to diminish when the observation depth increases. This could be explained by a possible inclination of the BHEs. The positions of the head of each BHEs is very well controlled, but their verticality is much more uncertain. In reality, an inclination of the BHEs can hardly be avoided. For instance Ref. [36], measured experimentally inclinations of BHEs up to 4% in a bedrock consisting mainly in a succession of siltstone/shale and sandstone layers while [71] measured inclinations up to 2% in a rock consisting in a succession of mudstone and sandstone layers). Those inclinations occur in rock materials, where the anisotropic character induced by the bedding planes can have a significant impact on the inclination of drilled BHEs. In soil materials, lower deviations can be expected. Consequently, the impact of an inclination from the vertical axis of 1% of the 3 non-activated boreholes was investigated. The activated BHE (F3) is supposed perfectly vertical and the three non-activated BHEs can have an inclination of 1% in all possible directions. An inclination of 1% produces a deviation of 0.58 m at the BOT level. Knowing the closest non-activated BHE is at 4.1 m from the activated BHE, it corresponds to an uncertainty of +/- 14% on the distance between them.

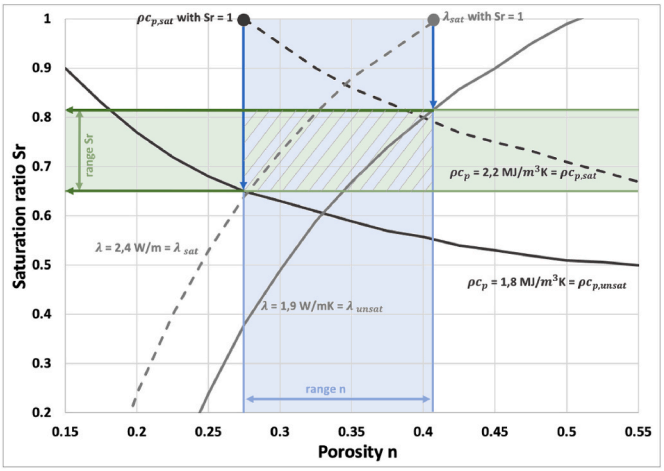

Fig. 11. Sets of porosity and degree of saturation corresponding to fixed values of thermal conductivity and volumetric heat capacity in both saturated and unsaturated parts of the Brusselian aquifer.

Table 5
Summary of the porosity and degree of saturation inferred from the thermal conductivity and volumetric heat capacity in the saturated part of the aquifer.

	Porosity n	Degree of saturation S_r
From thermal conductivity λ	0,41	0,82
From volumetric heat capacity ρc_p	0,28	0,65

In both unsaturated (i.e., TOP) and saturated domains (i.e., WAT and BOT), the simulations are based on the calibrated hydro-geothermal values displayed in Table 4. The possible range of predicted temperature evolutions are plotted in comparison with the experimental data on Figs. 12–14, at the TOP, WAT and BOT levels, respectively. The hypothesis of the possible slight inclination of the BHEs to explain the mismatching at greater depths between simulated and measured temperature evolutions is highly plausible. However, even an inclination of 1% does not allow to significantly reduce the gap between the simulated and monitored temperature curves within the F4 BHE at the BOT level (Fig. 14). As mentioned earlier, this significant gap could be also explained by an incorrect installation depth of the temperature sensors.

6. Conclusions

An experimental set-up to monitor the temperature field around an activated BHE was proposed, based on the insertion of temperature sensors at different depths in both an activated BHE and surrounding non-activated BHEs. Then a procedure to characterize the groundwater

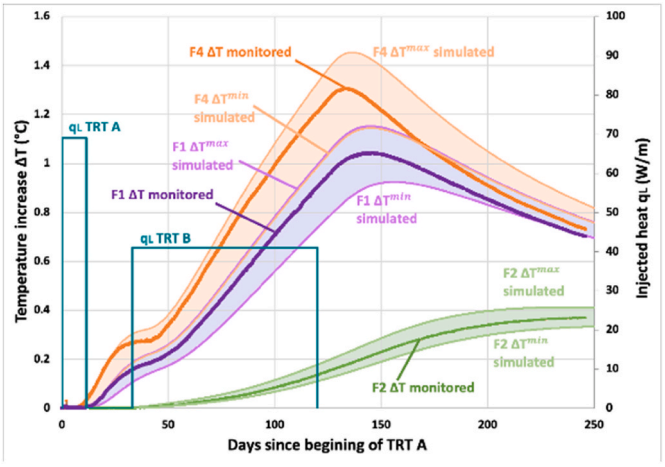

Fig. 12. Range of temperature for each non-activated BHE considering a possible inclination of 1% at the TOP level.

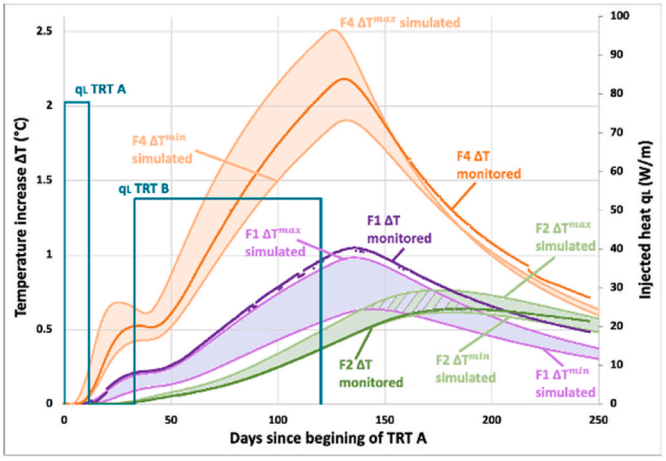

Fig. 13. Range of temperature for each non-activated BHE considering a possible inclination of 1% at the WAT level.

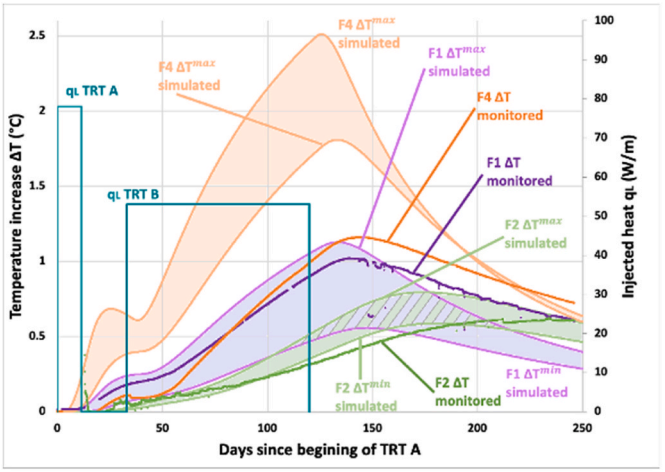

Fig. 14. Range of temperature for each non-activated BHE considering a possible inclination of 1% at the BOT level.

fluxes, the intrinsic thermal conductivity and the volumetric heat capacity of the ground from the monitoring of the thermal plume was developed. The procedure can be divided in 4 distinct steps: (i) design of duration and heat load of the heat injection within the activated BHE, (ii) sensitivity analysis of the different unknown parameters to discriminate the parameters that play a significant role on the temperature evolution at the near field (i.e. at the activated BHE) and in the far field (i.e. at the non-activated BHE), (iii) determination of selected hydro-geothermal parameters of the ground based on the temperature evolution within the activated BHE and (iv) determination of the remaining parameters based on the temperature evolution in the far field.

The calibration rests upon an analytical solution providing the temperature field around BHEs for discontinuous heat extraction, and based on the finite line source model considering conductive, advective and dispersive heat exchanges. The methodology was developed on an unconfined aquifer, for which the temperature field was monitored at three different depths in both the saturated and unsaturated parts. The different steps of the procedure were applied successively at the three different monitoring depths. Even if the procedure can be successfully applied on a temperature field characterized at a single depth, the collection of experimental temperatures at different depths in both saturated and unsaturated parts of the aquifer allow to reduce the number of unknowns of the problem, since some parameters such as the BHE thermal resistance can be reasonably assumed constant all along the BHE. So, combining information from both saturated and unsaturated parts of the unconfined aquifer allows to increase the robustness of the methodology, and in turn the reliability of the back-analyzed ground hydro-geothermal parameters around an activated BHE.

The application of the procedure showed that the calibrated hydro-geothermal parameters of the ground provide on average a good correlation between the monitored temperature and the predicted temperature evolutions. This good correlation was also supported by a blind prediction of the temperature evolution within a nearby piezometer. It also highlights the clear impact of groundwater fluxes on the temperature field around BHEs. This effect could become significant for a sustainable use of the ground heat reservoir.

The discrepancies between monitored and simulated temperatures tend nevertheless to increase at greater depths. This could be justified by (i) the inclination of the BHEs assumed to be vertical during the different simulations and (ii) an inaccuracy on the insertion depth of the temperature sensors at the bottom of the aquifer. The impact of a 1% inclination of the non-activated BHEs on the predicted temperatures within the BHEs was performed and demonstrates the relevance of this hypothesis. An accurate control of the vertical inclination of BHE is thus needed to carefully characterized the temperature field around an activated BHE.

Finally, the development of an automated calibration of the ground hydro-geothermal procedure based on a suitable minimization procedure and that would allow the identification of the best set of parameters could be envisaged as a perspective. Also, including in the calibration procedure the relationships that link the values of thermal conductivity and volumetric heat capacity between saturated and unsaturated domains of the aquifer would lead also to a reduction of the number of unknowns.

CRediT authorship contribution statement

Valériane Gigot: Conceptualization, Methodology, Formal analysis, Investigation, Validation, Visualization, Writing – original draft. **Bertrand Francois:** Funding acquisition, Methodology, Writing – review & editing, Supervision. **Marijke Huysmans:** Supervision, Writing – review & editing. **Pierre Gerard:** Funding acquisition, Methodology, Project administration, Supervision, Writing – review & editing.

Declaration of competing interest

The authors declare that they have no known competing financial interests or personal relationships that could have appeared to influence

the work reported in this paper.

Acknowledgments

This work was supported by the European Regional Development Fund (EDRF) and the Brussels Capital Region in the frame of the project F31-03 “Brugeo”. The authors would like also to thank Fabiano Pucci and Nicolas Canu for their valuable support for the experimental developments performed on the experimental platform.

References

[1] B. Sanner, Shallow Geothermal Energy, vol. 19, GHC Bulletin, June, 2001.
[2] W.J. Eugster, B. Sanner, Technological status of shallow geothermal energy in Europe, in: Proceedings European Geothermal Congress, vol. 8, 2007.
[3] G.A. Narsilio, L. Aye, Shallow geothermal energy: an emerging technology, in: A. Sharma, A. Shukla, L. Aye (Eds.), Low Carbon Energy Supply. Green Energy and Technology, Springer, Singapore, 2018, https://doi.org/10.1007/978-981-10-7326-7_18.
[4] R. Perego, G. Dalla Santa, A. Galgaro, S. Pera, Intensive thermal exploitation from closed and open shallow geothermal systems at urban scale: unmanaged conflicts and potential synergies, Geothermics 103 (2022), 102417, https://doi.org/10.1016/j.geothermics.2022.102417.
[5] D. Hillel, Environmental Soil Physics: Fundamentals, Applications, and Environmental Considerations, Elsevier, 1998.
[6] H. Jin, Y. Wang, Q. Zheng, H. Liu, E. Chadwick, Experimental study and modelling of the thermal conductivity of sandy soils of different porosities and water contents, Appl. Sci. 7 (2) (2017) 119, https://doi.org/10.3390/app7020119.
[7] D.A. Stonestrom, K.W. Blasch, *Determining Temperature and Thermal Properties for Heat-Based Studies of Surface-Water Ground-Water Interactions: Appendix A of Heat As a Tool for Studying the Movement of Ground Water Near Streams (Cir1260)* (No. Appendix A, Pp. 73-80), US Geological Survey, 2003.
[8] A. Casasso, R. Sethi, Efficiency of closed loop geothermal heat pumps: a sensitivity analysis, Renew. Energy 62 (2014) 737–746, https://doi.org/10.1016/j.renene.2013.08.019.
[9] D. Banks, A review of the importance of regional groundwater advection for ground heat exchange, Environ. Earth Sci. 73 (6) (2015) 2555–2565, https://doi.org/10.1016/j.renene.2019.05.092.
[10] H. Wang, C. Qi, H. Du, J. Gu, Thermal performance of borehole heat exchanger under groundwater flow: a case study from Baoding, Energy Build. 41 (12) (2009) 1368–1373, https://doi.org/10.1016/j.enbuild.2009.08.001.
[11] M.V. Klepikova, T. Le Borgne, O. Bour, P. Davy, A methodology for using borehole temperature-depth profiles under ambient, single and cross-borehole pumping conditions to estimate fracture hydraulic properties, J. Hydrol. 407 (1–4) (2011) 145–152, https://doi.org/10.1016/j.jhydrol.2011.07.018.
[12] J.C. Choi, J. Park, S.R. Lee, Numerical evaluation of the effects of groundwater flow on borehole heat exchanger arrays, Renew. Energy 52 (2013) 230–240, https://doi.org/10.1016/j.renene.2012.10.028.
[13] A. Funabiki, M. Oguma, T. Yabuki, T. Kakizaki, The effects of groundwater flow on vertical-borehole ground source heat pump systems, in: Engineering Systems Design and Analysis, American Society of Mechanical Engineers, 2014, V003T12A005, https://doi.org/10.1115/ESDA2014-20065, 45851.
[14] A. Angelotti, L. Alberti, I. La Licata, M. Antelmi, Energy performance and thermal impact of a Borehole Heat Exchanger in a sandy aquifer: influence of the groundwater velocity, Energy Convers. Manag. 77 (2014) 700–708, https://doi.org/10.1016/j.enconman.2013.10.018.
[15] J. Luo, J. Tuo, W. Huang, Y. Zhu, Y. Jiao, W. Xiang, J. Rohn, Influence of groundwater levels on effective thermal conductivity of the ground and heat transfer rate of borehole heat exchangers, Appl. Therm. Eng. 128 (2018) 508–516, https://doi.org/10.1016/j.applthermaleng.2017.08.148.
[16] X. Yu, H. Li, S. Yao, V. Nielsen, A. Heller, Development of an efficient numerical model and analysis of heat transfer performance for borehole heat exchanger, Renew. Energy 152 (2020) 189–197, https://doi.org/10.1016/j.renene.2020.01.044.
[17] R. Fan, Y. Jiang, Y. Yao, D. Shiming, Z. Ma, A study on the performance of a geothermal heat exchanger under coupled heat conduction and groundwater advection, Energy 32 (11) (2007) 2199–2209, https://doi.org/10.1016/j.energy.2007.05.001.
[18] J. Hu, An improved analytical model for vertical borehole ground heat exchanger with multiple-layer substrates and groundwater flow, Appl. Energy 202 (2017) 537–549, https://doi.org/10.1016/j.apenergy.2017.05.152.
[19] S. Cai, X. Li, M. Zhang, J. Fallon, K. Li, T. Cui, An analytical full-scale model to predict thermal response in boreholes with groundwater advection, Appl. Therm. Eng. 168 (2020), 114828, https://doi.org/10.1016/j.applthermaleng.2019.114828.
[20] K. Jiao, C. Sun, R. Yang, B. Yu, B. Bai, Long-term heat transfer analysis of deep coaxial borehole heat exchangers via an improved analytical model, Appl. Therm. Eng. 197 (2021), 117370, https://doi.org/10.1016/j.applthermaleng.2021.117370.
[21] L. Zhang, L. Zhao, L. Yang, H. Songtao, Analyses on soil temperature responses to intermittent heat rejection from BHEs in soils with groundwater advection, Energy Build. 107 (2015) 355–365. https://doi.org/10.1016/j.enbuild.2015.08.040.
[22] Z. Zhao, Y.F. Lin, A. Stumpf, X. Wang, Assessing impacts of groundwater on geothermal heat exchangers: a review of methodology and modelling, Renew. Energy 190 (2022) 121–147, https://doi.org/10.1016/j.renene.2022.03.089.
[23] D.C. Smith, A.C. Elmore, The observed effects of changes in groundwater flow on a borehole heat exchanger of a large scale ground coupled heat pump system, Geothermics 74 (2018), https://doi.org/10.1016/j.geothermics.2018.03.008, 240-426.
[24] L. Guo, J. Zhang, Y. Li, J. McLennan, Y. Zhang, H. Jiang, Experimental and numerical investigation of the influence of groundwater flow on the borehole heat exchanger performance: a case study from Tangshan, China, Energy Build. 248 (2021), 111199, https://doi.org/10.1016/j.enbuild.2021.111199.
[25] S. Gehlin, Thermal Response Test: Method Development and Evaluation, Doctoral dissertation, Luleå tekniska universitet, 2002.
[26] B. Sanner, Standards and Guidelines for UTES/GSHP wells and boreholes, in: 14th International Conference on Energy Storage Adana, 2018.
[27] H.S. Carslaw, J.C. Jaeger, *Conduction Of Heat in Solids* (No. 536.23, Clarendon Press, Oxford, UK, 1959. ISBN:978-0-19-853368-9.
[28] N. Diao, Q. Li, Z. Fang, Heat transfer in ground heat exchangers with groundwater advection, Int. J. Therm. Sci. 43 (12) (2004) 1203–1211, https://doi.org/10.1016/j.ijthermalsci.2004.04.009.
[29] A.D. Chiasson, S.J. Rees, J.D. Spitler, A Preliminary Assessment of the Effects of Groundwater Flow on Closed-Loop Ground Source Heat Pump Systems, Oklahoma State Univ., Stillwater, OK (US), 2000.
[30] P.E. Pehme, B.L. Parker, J.A. Cherry, J.W. Molson, J.P. Greenhouse, Enhanced detection of hydraulically active fractures by temperature profiling in lined heated bedrock boreholes, J. Hydrol. 484 (2013) 1–15, https://doi.org/10.1016/j.jhydrol.2012.12.048.
[31] P. Pehme, B.L. Parker, J.A. Cherry, D. Blohm, Detailed measurement of the magnitude and orientation of thermal gradients in lined boreholes for characterizing groundwater flow in fractured rock, J. Hydrol 513 (2014) 101–114, https://doi.org/10.1016/j.jhydrol.2014.03.015.
[32] T.I. Coleman, B.L. Parker, C.H. Maldaner, M.J. Mondanos, Groundwater flow characterization in a fractured bedrock aquifer using active DTS tests in sealed boreholes, J. Hydrol. 528 (2015) 449–462, https://doi.org/10.1016/j.jhydrol.2015.06.061.
[33] C.H. Maldaner, J.D. Munn, T.I. Coleman, J.W. Molson, B.L. Parker, Groundwater flow quantification in fractured rock boreholes using active distributed temperature sensing under natural gradient conditions, Water Resour. Res. 55 (4) (2019) 3285–3306, https://doi.org/10.1029/2018WR024319.
[34] C.H.K. Pambou, J. Raymond, L. Lamarche, Improving thermal response tests with wireline temperature logs to evaluate ground thermal conductivity profiles and groundwater fluxes, Heat Mass Tran. 55 (6) (2019) 1829–1843, https://doi.org/10.1007/s00231-018-2532-y.
[35] W.R. Lim, S.Y. Hamm, C. Lee, S. Hwang, I.H. Park, H.C. Kim, Characteristics of deep groundwater flow and temperature in the tertiary pohang area, South Korea, Appl. Sci. 10 (15) (2020) 5120, https://doi.org/10.3390/app10155120.
[36] G. Radioti, B. Cerfontaine, R. Charlier, F. Nguyen, Experimental and numerical investigation of a long-duration Thermal Response Test: borehole Heat Exchanger behaviour and thermal plume in the heterogeneous rock mass, Geothermics 71 (2018) 245–258, https://doi.org/10.1016/j.geothermics.2017.10.001.
[37] H. Schwarz, B. Badenes, J. Wagner, J.M. Cuevas, J. Urchueguía, D. Bertermann, A case study of thermal evolution in the vicinity of geothermal probes following a distributed TRT method, Energies 14 (9) (2021) 2632, https://doi.org/10.3390/en14092632.
[38] T. Hermans, S. Wildemeersch, P. Jamin, P. Orban, S. Brouyère, A. Dassargues, F. Nguyen, Quantitative temperature monitoring of a heat tracing experiment using cross-borehole ERT, Geothermics 53 (2015) 14–26, https://doi.org/10.1016/j.geothermics.2014.03.013.
[39] S. Erol, M.A. Hashemi, B. François, Analytical solution of discontinuous heat extraction for sustainability and recovery aspects of borehole heat exchangers, Int. J. Therm. Sci. 88 (2015) 47–58, https://doi.org/10.1016/j.ijthermalsci.2014.09.007.
[40] T. Coen, B. François, P. Gerard, Analytical solution for multi-borehole heat exchangers field including discontinuous and heterogeneous heat loads, Energy Build. 253 (2021), 111520, https://doi.org/10.1016/j.enbuild.2021.111520.
[41] J.W. Hopmans, J. Šimunek, K.L. Bristow, Indirect estimation of soil thermal properties and water flux using heat pulse probe measurements: geometry and dispersion effects, Water Resour. Res. 38 (1) (2002), https://doi.org/10.1029/2000WR000071, 7-1.
[42] A. Alkindi, Y. Al-Wahaibi, B. Bijeljic, A. Muggeridge, Investigation of longitudinal and transverse dispersion in stable displacements with a high viscosity and density contrast between the fluids, J. Contam. Hydrol. 120 (2011) 170–183, https://doi.org/10.1016/j.jconhyd.2010.06.006.
[43] J.M.P.Q. Delgado, Longitudinal and transverse dispersion in porous media, Chem. Eng. Res. Des. 85 (9) (2007) 1245–1252, https://doi.org/10.1205/cherd07017.
[44] S. Liu, J.H. Masliyah, Dispersion in porous media, Handbook of porous media 81 (2005) 140.
[45] J.S. Chen, C.W. Liu, C.P. Liang, Evaluation of longitudinal and transverse dispersivities/distance ratios for tracer test in a radially convergent flow field with scale-dependent dispersion, Adv. Water Resour. 29 (6) (2006) 887–898, https://doi.org/10.1016/j.advwatres.2005.08.001.
[46] J. Hecht-Méndez, M. De Paly, M. Beck, P. Bayer, Optimization of energy extraction for vertical closed-loop geothermal systems considering groundwater flow, Energy Convers. Manag. 66 (2013) 1–10, https://doi.org/10.1016/j.enconman.2012.09.019.

[47] N. Molina-Giraldo, P. Blum, K. Zhu, P. Bayer, Z. Fang, A moving finite line source model to simulate borehole heat exchangers with groundwater advection, Int. J. Therm. Sci. 50 (12) (2011) 2506–2513, https://doi.org/10.1016/j.ijthermalsci.2011.06.012.
[48] G. Hellström, Ground Heat Storage: Thermal Analyses of Duct Storage Systems, Lund University, 1991.
[49] J. Bennet, J. Claesson, G. Hellström, Multipole method to compute the conductive heat flows to and between pipes in a composite cylinder, Tech. Rep. 3-1987, Department of Building Physics, Lund Institute of Technology, Lund, Sweden (1987).
[50] C.P. Remund, Borehole thermal resistance: laboratory and field studies, Build. Eng. 105 (1999) 439.
[51] Y. Gu, D.L. O'Neal, Development of an equivalent diameter expression for vertical U-tubes used in ground-coupled heat pumps, Transactions-American Society of Heating Refrigerating and air Conditioning Engineers 104 (1998) 347–355.
[52] X. Devleeschouwer, C. Goffin, J. Vandaele, B. Meyvis, Modelisation stratigraphique en 3D du sous-sol de la Region de Bruxelles-Capitale, Institut Royal des Sciences Naturelles de Belgique, 2017, p. 110. Available on, [1].
[53] M. Agniel, Modélisation hydrogéologique en éléments finis du système phréatique bruxellois, Bruxelles-Environnement 147 (2020). https://environnement.br.ussels/thematiques/geologie-et-hydrogeologie/eaux-souterraines/modelisation/br.ussels-phreatic-system-model.
[54] A. Vieira, M. Alberdi-Pagola, P. Christodoulides, S. Javed, F. Loveridge, F. Nguyen, G. Radioti, Characterisation of ground thermal and thermo-mechanical behaviour for shallow geothermal energy applications, Energies 10 (12) (2017) 2044, https://doi.org/10.3390/en10122044.
[55] A. Zarrella, G. Emmi, S. Graci, M. De Carli, M. Cultrera, G.D. Santa, A. Bernardi, Thermal response testing results of different types of borehole heat exchangers: an analysis and comparison of interpretation methods, Energies 10 (6) (2017) 801, https://doi.org/10.3390/en10060801.
[56] CSTC, *Géothermie peu profonde - Conception et mise en œuvre de systèmes avec échangeurs en forme de U* . Note d'Information Technique 259, Centre Scientifique et Technique de la Construction. Bruxelles: CSTC, 2016.
[57] P. Gerard, M. Vincent, B. François, A methodology for lithology based thermal conductivity at a regional scale – application to the Brussels Capital Region, Geothermics 95 (2021), 102117, https://doi.org/10.1016/j.geothermics.2021.102117.
[58] S. Brouyère, J. Batlle-Aguilar, P. Goderniaux, A. Dassargues, A new tracer technique for monitoring groundwater fluxes: the Finite Volume Point Dilution Method, J. Contam. Hydrol. 95 (3–4) (2008) 121–140, https://doi.org/10.1016/j.jconhyd.2007.09.001.
[59] P. Jamin, P. Goderniaux, O. Bour, T. Le Borgne, A. Englert, L. Longuevergne, S. Brouyère, Contribution of the finite volume point dilution method for measurement of groundwater fluxes in a fractured aquifer, J. Contam. Hydrol. 182 (2015) 244–255, https://doi.org/10.1016/j.jconhyd.2015.09.002.
[60] S.E. Dehkordi, R.A. Schincariol, Effect of thermal-hydrogeological and borehole heat exchanger properties on performance and impact of vertical closed-loop geothermal heat pump systems, Hydrogeol. J. 22 (1) (2014) 189–203, https://doi.org/10.1007/s10040-013-1060-6.
[61] M. Le Lous, F. Larroque, A. Dupuy, A. Moignard, Thermal performance of a deep borehole heat exchanger: insights from a synthetic coupled heat and flow model, Geothermics 57 (2015) 157–172, https://doi.org/10.1016/j.geothermics.2015.06.014.
[62] M. Huysmans, L. Peeters, G. Moermans, A. Dassargues, Relating small-scale sedimentary structures and permeability in a cross-bedded aquifer, J. Hydrol. 361 (1–2) (2008) 41–51, https://doi.org/10.1016/j.jhydrol.2008.07.047.
[63] M. Possemiers, M. Huysmans, L. Peeters, O. Batelaan, A. Dassargues, Relationship between sedimentary features and permeability at different scales in the Brussels Sands, Geol. Belg. 15 (3) (2012) 156–164.
[64] P. Pasquier, D. Marcotte, Robust identification of volumetric heat capacity and analysis of thermal response tests by Bayesian inference with correlated residuals, Appl. Energy 261 (2020), 114394, https://doi.org/10.1016/j.apenergy.2019.114394.
[65] S. Signorelli, Geoscientific Investigations for the Use of Shallow Low-Enthalpy Systems, Doctoral dissertation, ETH Zurich, 2004.
[66] L. Laloui, A. Rotta Loria, Heat and mass transfers in the context of energy geostructures, Analysis and Design of Energy Geostructures 69 (2020) 135, https://doi.org/10.1016/B978-0-12-816223-1.00003-5.
[67] O. Johansen, Thermal Conductivity of Soils, Cold Regions Research and Engineering Lab Hanover NH, 1977.
[68] N. Zhang, Z. Wang, Review of soil thermal conductivity and predictive models, Int. J. Therm. Sci. 117 (2017) 172–183, https://doi.org/10.1016/j.ijthermalsci.2017.03.013.
[69] D. Lagrou, R. Dreesen, L. Broothaers, Comparative quantitative petrographical analysis of Cenozoic aquifer sands in Flanders (N Belgium): overall trends and quality assessment, Mater. Char. 53 (2–4) (2004) 317–326, https://doi.org/10.1016/j.matchar.2004.07.012.
[70] J.P. Dam, J. Nuyens, V. Roisin, R. Thonnard, Carte géotechnique 31.7.2. Bruxelles - Notice explicative. Commission de cartographie géotechnique, Institut Géotechnique de l'Etat, Belgium, 1984, p. 55.
[71] F.M. Wagner, P. Bergmann, C. Rücker, B. Wiese, T. Labitzke, C. Schmidt-Hattenberger, H. Maurer, Impact and mitigation of borehole related effects in permanent crosshole resistivity imaging: an example from the Ketzin CO2 storage site, J. Appl. Geophys. 123 (2015) 102–111, https://doi.org/10.1016/j.jappgeo.2015.10.005.